Progress In Electromagnetics Research, Vol. 115, 113–129, 2011

INVERSE MODELING IN APPLICATION FOR SEQUENTIAL FILTER TUNING

J. J. Michalski

TeleMobile Electronics Ltd.
Pomeranian Science and Technology Park, Gdynia, Poland

Abstract—This paper presents a new method of sequential microwave filter tuning. For filters with R tuning elements (including cavities, couplings and cross-couplings), based on physically measured scattering characteristics in the frequency domain, the Artificial Neural Network (ANN) is used to build inverse models of R sub-filters. Each sub-filter is associated to one tuning element. The sub-filters are obtained by successive opening or shorting of resonators and by removing coupling screws. For each sub-filter, the ANN training vectors are defined as physical reflection characteristics (input vectors) and the corresponding positions of the tuning element, which is detuned, in both directions, from its proper setting (output vectors). In the tuning process, such inverse models are used for calculating the tuning element increments needed for setting the tuning element in the proper position. The tuning experiment, conducted on 8- and 11-cavity filters, has shown the performance of the presented method.

1. INTRODUCTION

Although the methodologies for designing filters of various configurations have been known for decades, researchers are still introducing new solutions [1–8]. Depending on filter technology, frequency band and production quality filters have to be tuned or are ready for use directly after manufacturing. Filter tuning must be performed by experienced operators, which generates costs, and is a very important phase in production.

Filter tuning has been a very popular subject of research in the last couple of decades. All tuning methods can be divided into two main

Received 11 February 2011, Accepted 14 March 2011, Scheduled 23 March 2011
Corresponding author: Jerzy Julian Michalski (jerzy.michalski@telemobile.net.pl).

categories: parallel tuning and sequential tuning. In parallel tuning, like in the method proposed by Thal [22] and recently reported in [23] algorithms indicate which tuning elements cause filter detuning. The other one of the filter tuning categories is sequential tuning, where the tuning is performed successively from one filter side to another (usually from filter input to the output). The first sequential method was presented by Dishal in [9]. This method originally used a very loosely coupled detector attached to the first resonator in order to measure amplitude oscillograms. While analyzing voltage values on the center filter frequency, the tuning was performed from the filter input, where a generator was attached, to the filter output. For all odd-numbered resonators the maximum voltage, and for all even-numbered resonators the minimum voltage was observed on center frequency, in accordance with the input impedance changes (short, open, short etc.), while the successive resonators were being tuned. Next method was introduced by Atia and Williams in [10]. This method combines the concept of Dishal, with their methodology of measuring frequencies at which the phase of the input reflection coefficient is either 0° or 180°. This methodology was further developed by Chen [11]. In his approach, cavities and coupling tuning elements are adjusted sequentially one by one in accordance with the match of the measured input impedance to the resonance condition. In next method for sequential filter tuning [12] Ness, used group delay of the reflection coefficient. In this approach, group delay values at the center filter frequency must be set at the designed value sequentially for each cavity, while simultaneously maintaining the symmetry of the entire group delay characteristic. Modification of this method was proposed by Zahirovic and Mansour in [13]. The authors applied the derived group delay using Hilbert transformation of the transmission coefficient module. This method uses the module characteristic of the transmission. As a result, scalar network analyzers can be used instead of expensive vector network analyzers. Another approach was demonstrated by Dunsmore in [16], where tuning was carried out in the time domain. In this approach the time response of the tuned filter is compared to the response of properly tuned filter template in time domain, and tuning elements are sequentially set in proper positions. In elaboration [17] the authors present the tuning concept based on cloning the frequency domain data. The next method based on sequential parameter estimation was presented in [21]. In this work the authors presented an algorithm for computer-aided tuning, which prevents error propagation. A new system and method based on scalar measurement, applied for tuning of integrated tunable filters is reported in [24].

In recent works, the authors have introduced new methods based

on artificial intelligence algorithms (AI) not only in filter tuning but also in designing [18]. In [14, 15], the authors presented a method based on fuzzy logic system (FLS). Using linguistic expert rules, they proved that such an approach can be suitable for filter tuning. A novel approach based on ANN was presented in [25]. In this work, we proved that, thanks to multidimensional approximation ability of neural networks, unambiguous mapping between detuned filter characteristic and tuning element deviations which caused such detuning is possible. The method of improving efficiency of this approach [25] by using numerous golden filters was presented in [26]. Considering all the results obtained using the methods based on AI, continuation of such research seems very promising.

This paper presents a new sequential tuning method, based on ANN applied for cavity filters. For filters having R tuning elements, including cavities, couplings and cross-couplings, we have built R inverse sub-filter models which are modeled by ANN. The training set for each sub-filter is prepared in such a way that the tuning element is slightly detuned, in both directions, from its proper position. During this process, the training vectors consisting of reflection characteristics and corresponding tuning element deviations are collected. After the training process, the ANN, for each sub-filter, and for the detuned reflection characteristic, generates the tuning element increment, which is needed to set the tuning element in a proper position. If the tuning element increment generated by ANN equals zero, it indicates that the proper tuning element position has been reached. Then, the next tuning step is performed, and the next tuning element (inverse model) is taken.

In the first part of the paper, the general concept and the methodology of constructing inverse models are presented. Next, tuning experiments for 8- and 11-cavity filters are demonstrated. The summary and relevant remarks are presented at the end of the paper.

2. GENERAL CONCEPT

In general, transmission and reflection characteristics of two-port filter network, composed of a series of N inter-coupled resonators can be defined as a ratio of two polynomials [19, 20].

$$S_{11}(\omega) = \frac{F_N(\omega)}{E_N(\omega)};\ S_{21}(\omega) = \frac{P_N(\omega)}{\varepsilon E_N(\omega)} \tag{1}$$

where ω represents angular frequency and ε denotes constant normalizing of S_{21} to the equiripple level. The degree of common denominator $E(\omega)$ and S_{11} numerator $F(\omega)$ is N, and the degree of $P(\omega)$ corresponds to the number of non-infinite transmission zeros.

For a physical filter, scattering characteristics are adjusted by its tuning elements. The number of tuning elements depends on filter topology, the number of resonators, tunable couplings and cross-couplings. For synchronously coupled N cavity filters, the number of tuning elements is usually $R = 2N+1$. For filters with cross-couplings, this number is increased by the number of tuning elements responsible for adjusting the transmission zeros.

2.1. Sequential Inverse Modeling of the Filter Sub-filters

The reflection characteristic of the filter with R tuning elements can be generally expressed as a function of all tuning element deviations (including coupling tuning elements)

$$S_{11}(\omega) = H(\omega,\ \Delta Z_1,\ \Delta Z_2,\ \ldots,\ \Delta Z_R) \tag{2}$$

In our further analysis, we assume that the function describing the reflection characteristic is defined in such a way that, for all tuning element deviations equal zero $\Delta Z_n = 0$, it represents the characteristics S_{11}^0 of a properly tuned filter

$$S_{11}^0(\omega) = H(\omega,\ 0,\ 0, \ldots,\ 0) \tag{3}$$

The main concept of the presented method is to use a properly tuned physical filter as a template to build R sub-filter inverse models. For a filter having R tuning elements as the rth sub-filter, we define the filter having $1, 2, \ldots, r-1$, tuning elements properly tuned and the elements $r+1, \ldots, R$ removed or short-circuited. In such case, only the rth tuning element can be changed for adjusting of reflection characteristics (Figure 1).

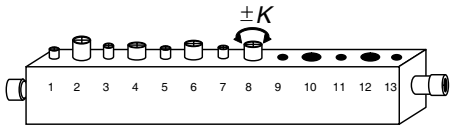

Figure 1. The 8th sub-filter model of $N = 6$ cavities, $R = 13$ tuning elements filter. The tuning elements 1–7 are tuned, 9–13 are removed.

The inverse models, for all R sub-filters, are built based on physically measured reflection characteristics, generally described by (1). In the process of building inverse models, we start from the Rth tuning element (the last tuning element at the filter output). For every rth sub-filter we create $(2K + 1)$ training vectors as a set of the following pairs $P_n = \left\{S_n^k, \Delta Z_n^k\right\}$, where

$\Delta Z_n^k = \{-K, -K+u, -K+2u \ldots, \ 0, \ldots, \ K-2u, K-u, K\}$. The value of u defines the minimal angle change in (deg) of each of the tuning elements.

The value of K is the multiple value of u and defines the maximum tuning element increment in both directions. Both u and K values depend on sensitivity of physical tuning elements and should be chosen experimentally. For each rth sub-filter, with $\Delta Z_r = 0$, S_r^0 represents proper scattering characteristics (the pattern in the tuning process). After creating the P_r set, if the rth tuning element is a coupling, its tuning element needs to be removed from the filter; while if it is a cavity depending on inverse model assumption, it needs be removed or short-circuited. Then, the next P_{r-1} set for (r-1) sub-filter model can be created. After creating the last sub-filter set P_1, all the tuning elements are removed or short-circuited. For every set P_r, we create the operator A_r: $S(Z_r) \rightarrow \Delta Z_r$ which maps detuned $S(Z_r)$ characteristic to the tuning element value ΔZ_r which has caused the detuning. In our approach, the operator A_r is modeled by artificial neural network ANNr. The characteristics S_r^k (real and imaginary part) and ΔZ_r^k are used respectively as ANNr input vectors and as ANNr output vectors in the training process. For each sub-filter model, and for each reflection characteristic S_r being used for building A_r operator, the following definition of error (4) is applied to check the ANN learning ability during the ANN training process

$$L_r = \frac{\sum_{k=1}^{2K+1} \left|\Delta Z_r^{k_0} - \Delta Z_r^{k_x}\right|}{2K+1} \quad [u] \tag{4}$$

where r — sub-filter model number, k — tuning element increment index, $\Delta Z_r^{k_0}$ — the correct value of the tuning element increment, $\Delta Z_r^{k_x}$ — the tuning element increment value generated by ANN, both for the corresponding S_r^k. After ANN$_r$ is trained, it works for the rth sub-filter as the mapper of measured detuned reflection characteristic S_r^* to the tuning element increment ΔZ_r, which is the source of the detuning (Figure 2).

This method possesses numerous attractive features. One of them,

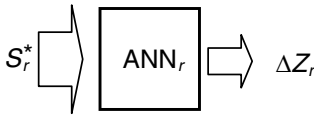

Figure 2. ANN generating tuning element deviation, which is the source of detuning, for the detuned scattering reflection characteristic for rth sub-filter.

which ought to be highlighted, is that, the inverse models are built based on the characteristic of physical filters. We have used the same environment both for building the inverse models and for tuning. Moreover, because reflection measurements are very sensitive to losses, in the presented approach we can build inverse models from both filter sides, detuning the filter from its middle towards the filter input and output. Such mechanism will be presented below, in the experiment for an 8-cavity filter.

2.2. Tuning Procedure

During the tuning process, the tuning screws (cavities, couplings and cross-couplings) are set one by one, in order to match (in the meaning of the ANN network generalization) scattering (real and imaginary) reflection characteristics for all R inverse sub-models. The cavity tuning elements must be treated in the same way as in the process of building the inverse models, but all coupling tuning elements must be removed from the filter. For the rth tuning element, we use the A_r operator, which models the rth sub-filter. The tuning process starts, from the filter input, with the first tuning element. We use the A_1 operator which, for the measured detuned sub-filter characteristic S_1, generates the tuning element increment $A_1 : S_1(Z_1) \rightarrow \Delta Z_1$. The increment ΔZ_1, after the application on the tuning element Z_1, sets the tuning element in the proper position $Z_1+\Delta Z_1$, thus obtaining a proper scattering characteristic $S_1^0 = f(Z_1+\Delta Z_1)$ for the 1st sub-filter. If the tuning element is set in a proper position, A_1 will generate $\Delta Z_1 = 0$. When the first tuning element is properly set, we use the second A_2 operator which, for filter reflection characteristics S_2, returns ΔZ_2. We adjust the second set of tuning elements to achieve the ANN_2 response $\Delta Z_2 = 0$. Having adjusted in this way, successively, all the tuning elements from filter input to its output, we can regard the tuning process is completed.

3. NEURAL NETWORK ARCHITECTURE

There are many techniques that can realize multidimensional approximation, in our case the process of mapping the filter scattering characteristic S to tuning element deviations ΔZ. Artificial neural networks can be successfully used for this task [27].

In this approach, a 3-layer feed-forward (FF) network architecture (input, hidden and output layer) has been chosen. As we always consider only one tuning element at the time (contrary to the method presented in [25, 26]) the output layer has only one neuron. The

number of neurons, in the hidden layer, must be chosen experimentally as a compromise between learning time and learning/generalization ability of the network. In our experiment presented further we specified 5 hidden neurons.

As presented in (1), in general, transmission and reflection characteristics of a two-port filter network, composed of a series of N inter-coupled resonators can be defined as a ratio of two polynomials

$$S(\omega) = \frac{A(\omega)}{B(\omega)} = \frac{\sum_{i=0}^{M} a_i \omega^i}{\sum_{j=0}^{N} b_j \omega^j} \tag{5}$$

This equation can be transformed into

$$\sum_{i=0}^{M} a_i \omega^i = S(\omega) \sum_{j=0}^{N} b_j \omega^j \tag{6}$$

and in matrix form it can be written as

$$X_{L\times(M+1)} a_{(M+1)\times 1} - Y_{L\times(N+1)} b_{(N+1)\times 1} = 0 \tag{7}$$

and then

$$\left[X_{L\times(M+1)} - Y_{L\times(N+1)}\right] \begin{bmatrix} a_{(M+1)\times 1} \\ b_{(N+1)\times 1} \end{bmatrix} = 0 \tag{8}$$

which gives the final matrix form of homogeneous linear equation

$$Z_{L\times(M+N+2)} d_{(M+N+2)\times 1} = 0 \tag{9}$$

Last Equation (9) can be solved is if $S(\omega)$ characteristic (5) is sampled in at least $L \geq N + M + 2$ points. If we consider reflection characteristic S_{11}, then $M = N$ [19]. Having such discrete set of $S_l(\omega_l)$, $l = 1, 2, \ldots L$, we can, using these points, restore the whole characteristic in an analytical form. Considering this, we assume that for $L \geq 2(N + 1)$, unambiguous mapping between reflection characteristic S_{11} sampled at L points to tuning element positions is possible. Each sampled complex point of reflection characteristic requires two input neurons, one for real and the second for the imaginary part this gives us dependence between filter order N and number of input layer neurons $WI \geq 2L$.

3.1. Advantages of ANN Direct Mapping of Scattering Characteristics to the Position of Tuning Element

The method proposed in this paper has one very important feature. The operator $A : S(Z) \rightarrow \Delta_Z$ generates the zero value for one unique set of each tuning element.

In this part of the paper, we will compare the results of two methods which generate the error of tuning elements, indicating to

what extent the filter characteristic is detuned. The first one will be the method introduced by us and the second is the method based on error definition specified by† (10). S_r^0 defines tuned, and S_r^d detuned filter characteristics respectively

$$c = \sum_l^L \left(\left| \mathfrak{Re} S_r^0(l) - \mathfrak{Re} S_r^d(l) \right|^2 + \left| \mathfrak{Tm} S_r^0(l) - \mathfrak{Tm} S_r^d(l) \right|^2 \right) \quad (10)$$

where L is the number of samples of filter characteristic.

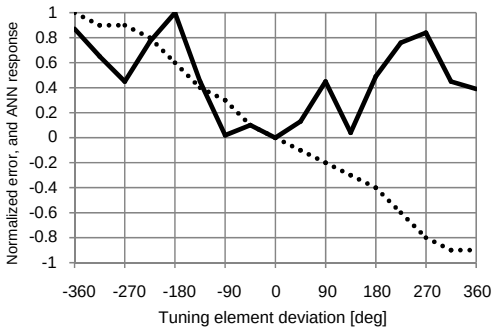

Figure 3. An exemplary normalized error defined by (10) (solid line) and normalized ANN response (dotted line) as a function of tuning element deviations.

Figure 3 presents the error defined by (10) (solid line) and the ANN response (dotted line) for different sets of tuning element. The curves are normalized to their maximum value. While analyzing them we can observe that the error curve generated by dependence (10) has numerous local minima, which can lead to setting the tuning element in an improper position. Looking at the ANN response, we can infer that it always describes unambiguously the proper tuning element position.

4. TUNING EXPERIMENT

In order to present the concept in practice, tuning experiments have been performed. Below, we present the tuning experiment results for two different filters. The first one is an 11-cavity cross-coupled filter with self-locking screws (Figure 4) and the second one is an 8-cavity cross-coupled filter with standard tuning screws with nuts (Figure 8).

† Similar error function was used in [21] to extract initial parameters of the sub-filter.

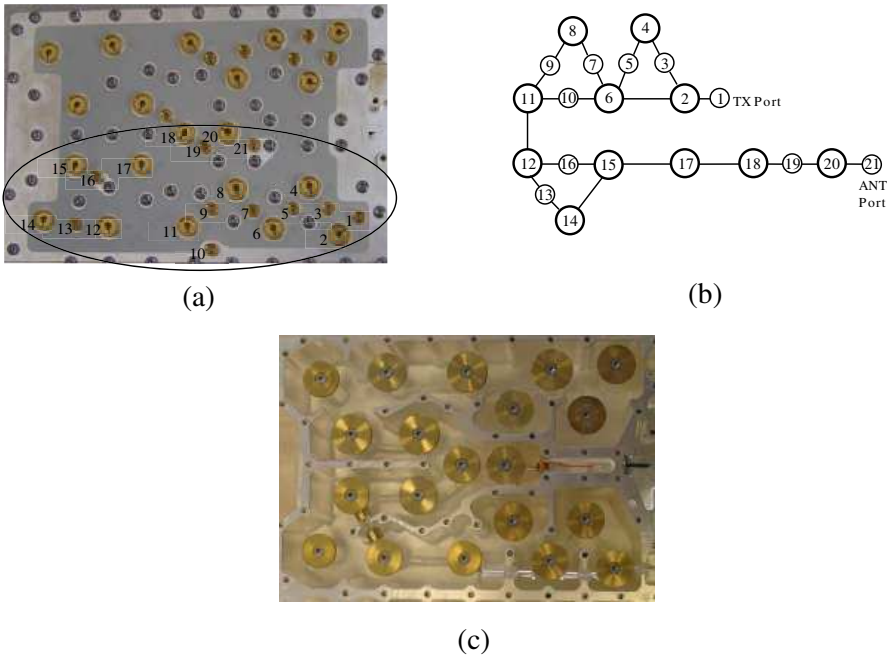

Figure 4. Layout (a), (c) and topology (b) of the filter used in the experiment. Small circles represent tunable coupling and cross-couplings. Bigger circles represent cavities. There are no coupling tuning elements between cavities 15–17, 17–18. Fixed cross-coupling occurs between cavities 2–6.

4.1. Self-locking Screws, 11-cavity Filter with Tunable Cross-couplings

The device tuned is an 11-cavity filter (the TX part of GSM diplexer) with 10 tunable couplings (Figure 4). The unit has self-locking screws. The cavities are represented by larger circles and the couplings and cross-couplings by the smaller ones. One fixed cross-coupling occurs between cavities 2–6 and two tunable cross-couplings are present between cavities 6–11 and 12–15. There are no tuning elements between cavities 15–17 and 17–18. The center frequency of the filter is $f_0 = 943.5\,\text{MHz}$ and the bandwidth $\Delta f = 35\,\text{MHz}$. The technical filter specification requires that the reflection characteristic level should be within the passband below $-18\,\text{dB}$. The ANN training sets P_r are prepared by manual change of tuning elements. In the experiment we used $1u = 360°/16 = 22.5°$ and $K = 20$. The reflection characteristics were sampled at 256 complex points. The

tuning elements were extracted, for both cavities and couplings, for all sub-filters, after collecting the ANN training set P_r. The inverse models were built based on the following tuning elements extraction path: $21, 20, 19, \ldots, 2, 1$. It means that the tuning was performed in the opposite direction $1, 2, 3, \ldots, 20, 21$. In our experiment, the inverse filter models were built based on the reflection characteristics collected from one filter, which can be described as an inverse model template (IMT). The tuning process was performed for another filter of the same type, which shall be defined as a tuned filter (TF). The tuning process consisted of 21 sequential steps, which is the number of tuning elements. The scattering characteristics, measured during the chosen tuning steps are depicted in Figures 5–7. In all figures, the properly tuned characteristics of the IMT, which serve as individual sub-filter templates, are represented by solid lines. The characteristics of the TF are represented by dotted lines. Figure 5(a) presents the real part of the reflection characteristic in the situation when all tuning elements are removed from the filter. The corresponding reflection and transmission characteristics in (dB) are depicted in Figure 5(b).

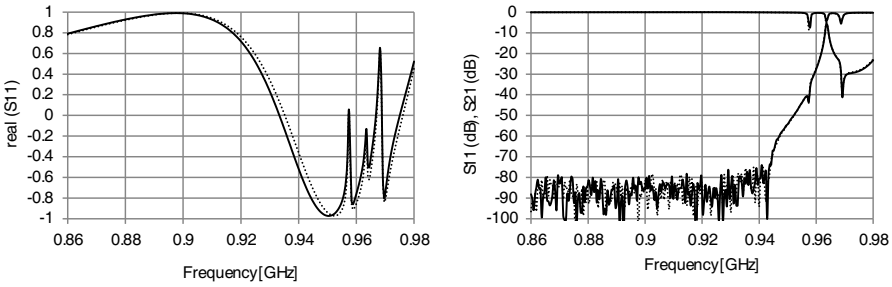

(a) (b)

Figure 5. (a) Real part of reflection. All tuning elements, 1–21, are removed. Solid line — IMT characteristic, dotted line — TF characteristic. (b) Transmission and reflection in (dB). All tuning elements, 1–21, are removed. Solid line — IMT, dotted line — TF characteristics.

The scattering characteristics, on completion of the 11th step of tuning, when 5 resonators are properly tuned, are presented in Figures 6(a), (b). Finally, the reflection characteristics on completion of the whole tuning process are presented in Figures 7(a), (b). We can observe that, since the tuned characteristics fulfill technical requirements, the tuning was performed successfully. If we start with all tuning elements extracted, the tuning time for this filter is about 5 minutes. While testing 5 other filters of the same type, we

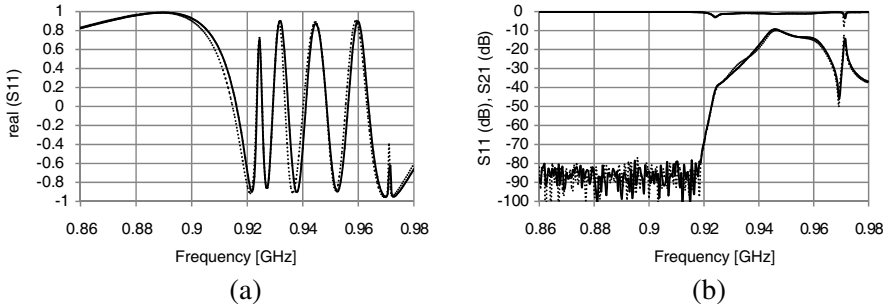

(a) (b)

Figure 6. (a) Real part of reflection. Tuning elements, 1–11, are tuned. Solid line — IMT characteristic, dotted line — TF characteristic. (b) Transmission and reflection in (dB). Tuning elements, 1–11, are tuned. Solid line — IMT characteristics, dotted line — TF characteristics.

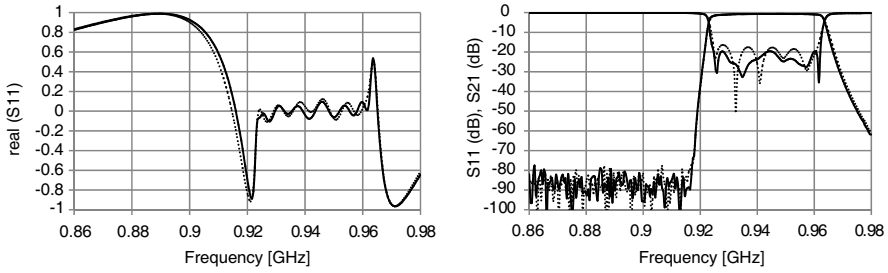

(a) (b)

Figure 7. (a) Real part of reflection. All tuning elements, 1–21, are tuned. Solid line — IMT characteristic, dotted line — TF characteristic. (b) Transmission and reflection in (dB). All tuning elements, 1–21, are tuned. Solid line — IMT, dotted line — TF characteristics.

observed that the return loss was, in all cases, below −16 dB. For some filters additional fine tuning is required. The paper [26] presents the method of improving tuning efficiency, which can also be applied in this approach.

4.2. Standard Screws, 8-cavity Filter with Fixed Cross-couplings

The next filter tuned is an 8-cavity cross-coupled filter with standard tuning screws with nuts (Figure 8). The filter was originally used as an

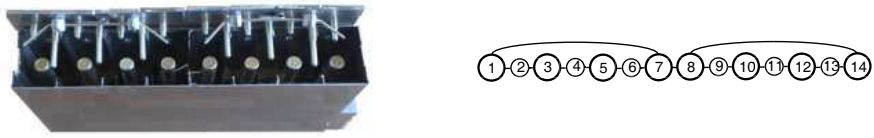

(a) (b)

Figure 8. The picture (a) and topology (b) of the filter used in the experiment. Small circles represent tunable couplings and cross-couplings. Bigger circles represent cavities. There is no tunable coupling element between cavities 7–8. Fixed cross-couplings can be found between the cavities 1–7 and 8–14.

RX filter in GSM combiner. The filter has two fixed cross-couplings, one between cavities 1–7 and the second one between cavities 8–14. There is no coupling tuning element between cavities 7–8. The center frequency of the filter is $f_0 = 897.5\,\mathrm{MHz}$ and the bandwidth $\Delta f = 35\,\mathrm{MHz}$. The technical filter specification requires that the reflection characteristic level should be within the passband below $-16\,\mathrm{dB}$. The ANN training sets P_r are prepared by manual change of tuning elements. In the experiment we used $1u = 360°/8 = 45°$ and $K = 10$. The sub-filters were built in such a way that the tuning elements were extracted from the filter center, in both directions, to its input and output. The inverse models were built based on the following tuning element extraction path: 8, 7, 9, 6, 10, 5, 11, 4, 12, 3, 13, 2, 14, 1. The inverse models were built based on reflection characteristic sampled at 32 complex points. Similarly to the previous diplexer tuning, in this experiment the filter inverse models were built based on the reflection characteristic collected from a different filter (inverse model template -IMT), than the one which was being tuned (TF). In all cases the characteristics for both filters are presented in figures. Below we present the filter characteristic obtained during the tuning process. Figures 9(a) and 9(b) present filter reflection and transmission characteristics with all tuning elements extracted. The discrepancies between characteristics of IMT and TF are caused by inaccuracies of filter production. These filters were intentionally chosen to demonstrate the reliability of the presented tuning method. The next curves, presented in Figures 10(a) and 10(b) show the situation on completion of the 10th tuning step, where elements 1–5 and 10–14 are properly set.

The last characteristics, depicted in Figures 11(a) and 11(b), show the filter condition on completion of the tuning, with all elements set. The tuning time for this filter, is about 3 minutes. It includes one tuning iteration, where each tuning element is positioned only once.

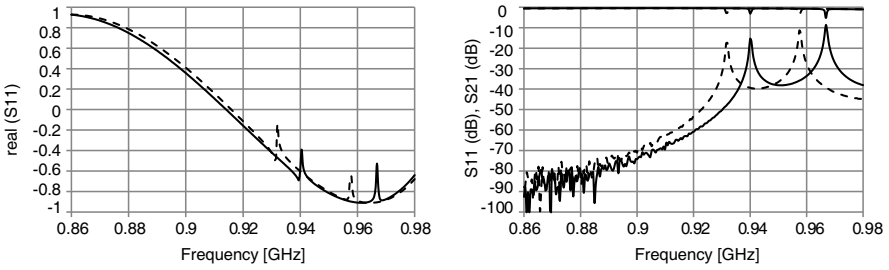

Figure 9. (a) Real part of reflection. All tuning elements, 1–14, are removed. Solid line — IMT characteristic, dotted line — TF characteristic. (b) Transmission and reflection in (dB). All tuning elements, 1–14, are removed. Solid line — IMT, dotted line — TF characteristics.

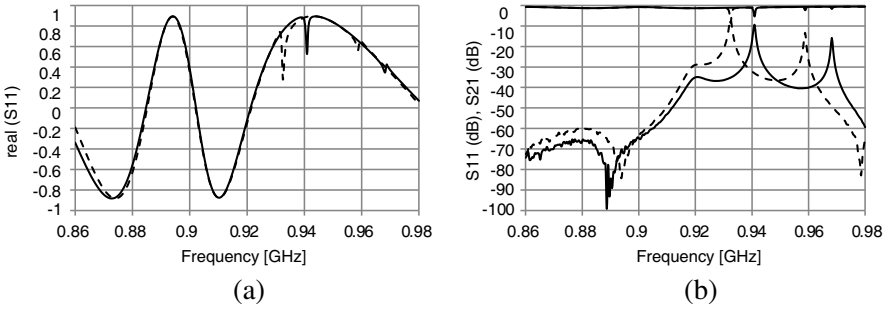

Figure 10. (a) Real part of reflection. Tuning elements, 1–5, 10–14 are tuned. Solid line — IMT characteristic, dotted line — TF characteristic. (b) Transmission and reflection in (dB). Tuning elements, 1–5, 10–14 are tuned. Solid line — IMT characteristics, dotted line — TF characteristics.

Due to filter discrepancy in some cases filter characteristics differ a little from specified tuning goals and the filter requires fine tuning, which can be performed very easily without any algorithm support and tuner's experience.

4.3. Advantages and Drawbacks of the Method in Comparison with Time Domain Approach

To check how effective the proposed method is, we tuned again the filters tuned in the experiment using time domain approach (TDA) [16]. The TDA results were not so satisfactory. Reflection characteristics

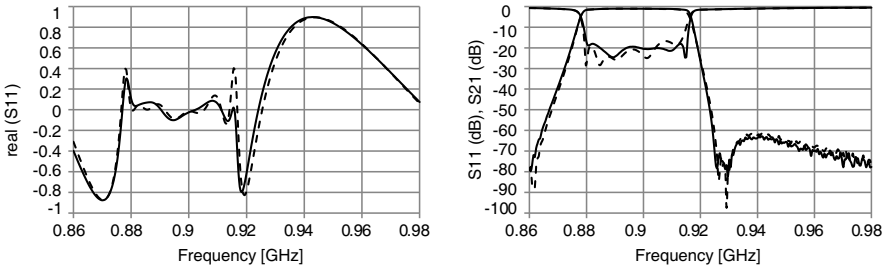

(a) (b)

Figure 11. (a) Real part of reflection. All tuning elements, 1–14, are tuned. Solid line — IMT characteristic, dotted line — TF characteristic. (b) Transmission and reflection in (dB). All tuning elements, 1–14, are tuned. Solid line — IMT, dotted line — TF characteristics.

in pass band, after one iteration, achieved the level of −10 dB only, and in the next iterations it was very difficult to improve the result. The existence of cross-couplings in both filters could be the main reason of this phenomenon. It is a well-known fact that time domain approach does not work well with cross-coupled filters. The drawbacks of our method includes the necessity of building as many ANN inverse models as many tuning elements are in the filter. Using robots for this purpose makes this process fully automatic, whilst the algorithms after customization can be used in both automated and manual tuning.

5. CONCLUSION

The new sequential filter tuning method based on artificial neural network inverse modeling in a frequency domain has been proposed. We have shown that the method of ANN direct mapping of detuned filter characteristic to tuning element error is very effective even in case of cross-coupled filters. Although the tuning experiments were demonstrated for the filters with all tuning elements extracted before tuning, the method can be applied, with short-circuited cavities, during the preparation of sub-filter inverse models and then in the tuning process. In the experiment, the filters were terminated with the matching load at output. The method can be successfully applied to filters terminated with open or short-circuit load. Although the method was demonstrated based on reflection characteristics, it can be customized with regard to any filter characteristics constituting the filter tuning goal. In order to demonstrate flexibility of this

approach, all learning samples are collected manually and all tuning experiments are performed manually. Nevertheless, this method can also be successfully applied for automated filter tuning.

ACKNOWLEDGMENT

This work was supported by National Ministry for Science & Higher Education (Decision nr. 736/N-COST/2010/0), under the project name "New optimization methods and their investigation for the application to physical microwave devices that require tuning" performed within the COST Action RFCSET IC0803.

REFERENCES

1. Razalli, M. S., A. Ismail, M. A. Mahdi, and M. N. Hamidon, "Novel compact 'via-less' ultra-wide band filter utilizing capacitive microstrip patch," *Progress In Electromagnetics Research*, Vol. 91, 213–227, 2009.
2. Mo, S. G., Z. Y. Yu, and L. Zhang, "Design of triple-mode bandpass filter using improved hexagonal loop resonator," *Progress In Electromagnetics Research*, Vol. 96, 117–125, 2009.
3. Ye, C. S., Y. K. Su, M. H. Weng, C. Y. Hung, and R. Y. Yang, "Design of the compact parallel-coupled lines wideband bandpass filters using image parameter method," *Progress In Electromagnetics Research*, Vol. 100, 153–173, 2010.
4. Zhang, L., Z.-Y. Yu, and S.-G. Mo, "Novel planar multimode bandpass filters with radial-line stubs," *Progress In Electromagnetics Research*, Vol. 101, 33–42, 2010.
5. Huang, J.-Q. and Q.-X. Chu, "Compact UWB band-pass filter utilizing modified composite right/left-handed structure with cross coupling," *Progress In Electromagnetics Research*, Vol. 107, 179–186, 2010.
6. Chiou, Y.-C., P.-S. Yang, J.-T. Kuo, and C.-Y. Wu, "Transmission zero design graph for dual-mode dual-band filter with periodic stepped-impedance ring resonator," *Progress In Electromagnetics Research*, Vol. 108, 23–36, 2010.
7. Lopez-Garcia, B., D. V. B. Murthy, and A. Corona-Chavez, "Half mode microwave filters based on epsilon near zero and mu near zero concepts," *Progress In Electromagnetics Research*, Vol. 113, 379–393, 2011.
8. Vegesna, S. and M. Saed, "Novel compact dual-band bandpass

microstrip filter," *Progress In Electromagnetics Research B*, Vol. 20, 245–262, 2010.

9. Dishal, M., "Alignment and adjustment of synchronously tuned multiple-resonant-circuit filters," *Proc. IRE*, Vol. 39, No. 11, 1448–1455, Nov. 1951.
10. Atia, A. E. and A. E. Williams, "Measurements of intercavity couplings," *IEEE Transactions Microwave Theory and Techniques*, Vol. 23, No. 6, 519–522, Jun. 1975.
11. Chen, M. H., "Short-circuit tuning method for singly terminated filters," *IEEE Transactions Microwave Theory and Techniques*, Vol. 25, No. 12, 1032–1036, Dec. 1977.
12. Ness, J. B., "A unified approach to the design, measurement, and tuning of coupled-resonator filters," *IEEE Transactions Microwave Theory and Techniques*, Vol. 46, 343–351, 1998.
13. Zahirovic, N. and R. R. Mansour, "Sequential tuning of coupled resonator filters using Hilbert transform derived relative group delay," *2008 IEEE MTT-S International Microwave Symposium Digest*, 739–742, Jun. 15–20, 2008.
14. Miraftab, V. and R. R. Mansour, "Tuning of microwave filters by extracting human experience using fuzzy logic," *2005 IEEE MTT-S International Microwave Symposium Digest*, 4, Jun. 12–17, 2005.
15. Miraftab, V. and R. R. Mansour, "Fully automated RF/microwave filter tuning by extracting human experience using fuzzy controllers," *IEEE Trans. on Circuits and Systems*, Vol. 55, No. 5, Jun. 2008.
16. Dunsmore, J., "Tuning band pass filters in the time domain," *IEEE MTT-S Int. Microwave Symp. Digest*, 1351–1354, 1999.
17. Lindner, A., H. Kugler, and E. Biebl, "Manual filter tuning by cloning frequency domain data," *37th European Microwave Conference 2007*, 329–331, Sep. 2007.
18. Kabir, H., Y. Wang, M. Yu, and Q.-J. Zhang, "Neural network inverse modeling and applications to microwave filter design," *IEEE Transactions on Microwave Theory and Techniques*, Vol. 56, No. 4, 867–879, Apr. 2008.
19. Cameron, R. J., C. M. Kudsia, and R. R. Mansour, *Microwave filter for Communication Systems: Fundamentals, Design, and Application*, John Wiley & Sons, Inc., 2007.
20. Cameron, R. J., "General coupling matrix synthesis methods for Chebyshev filtering functions," *IEEE Transactions on Microwave Theory and Techniques*, Vol. 47, No. 4, 433–442, Apr. 1999.

21. Pepe, G., F.-J. Gortz, and H. Chaloupka, "Sequential tuning of microwave filters using adaptive models and parameter extraction," *IEEE Transactions Microwave Theory and Techniques*, Vol. 53, No. 1, 22–31, Jan. 2005.
22. Thal, H. L., "Computer-aided filter alignment and diagnosis," *IEEE Transactions on Microwave Theory and Techniques*, Vol. 26, No. 12, 958–963, Dec. 1978.
23. Meng, M. and K.-L. Wu, "An analytical approach to computer-aided diagnosis and tuning of lossy microwave coupled resonator filters," *IEEE Transactions on Microwave Theory and Techniques*, Vol. 57, No. 12, 3188–3195, Dec. 2009.
24. Zahirovic, N., R. R. Mansour, and M. Yu, "Scalar measurement-based algorithm for automated filter tuning of integrated Chebyshev tunable filters," *IEEE Transactions Microwave Theory and Techniques*, Vol. 58, No. 12, 3749–3759, Dec. 2010.
25. Michalski, J., "Artificial neural networks approach in microwave filter tuning," *Progress In Electromagnetics Research M*, Vol. 13, 173–188, 2010.
26. Michalski, J., "Artificial neural network algorithm for automated filter tuning with improved efficiency by usage of many golden filters," *Proceedings of XVIII International Conference on Microwave, Radar and Wireless Communications MIKON-2010*, Vol. 3, 264–266, Lithuania, Vilnius, Jun. 14–16, 2010.
27. Haykin, S., *Neural Networks: A Comprehensive Foundation*, Prentice Hall, Upper Saddle River, NJ, 1999.